nature photonics

Article https://doi.org/10.1038/s41566-024-01413-2

# Turnkey locking of quantum-dot lasers directly grown on Si

In the format provided by the authors and unedited

## CONTENTS

## I. DEVICE FABRICATIONS

The active region consists of 5 layers of InAs quantum dots (QDs), which are buried in an InGaAs dot-in-a-well (DWELL) structure. The typical height of the dots is 5 nm and the base diameter is about 20 nm, which yields a tensile strain ranging from 3 $\sim$ 5% [1]. The dot density is $6{\times}10^{10}$cm$^{-2}$ (Fig. S1a). The photoluminescence wavelength of the ground state (GS) peak is close to 1300 nm and the full-width-at-half-maximum (FWHM) is narrower than 30 meV (Fig. S1b). The 37.5 nm spacer layer between each dot layer contained 10 nm-thick p-type GaAs to bring an extra 10 holes per dot for the improvement of thermal stability. Figure S2 depicts the full processing flow for the device fabrication. After completing the laser growth with the buried DFB grating structures (Inset in Fig. S3b), the materials were deeply etched down to the bottom n-contact layer to form the mesa structures with widths ranging from 1.7 to 3 $\mu m$. P- and N-contact vias were then opened after the first passivation for contact metal deposition. The device structure is then finished by depositing the probe metals after opening the vias in the second passivation layer. The as-fabricated on-Si devices were thinned to 200 $\mu m$ and then cleaved to form the laser facets. Detailed information about the epi-structure is summarized in Tab. I. It should be noted that our optimized regrowth process allows for reducing the growth defects in the p-cladding layer. A comparison of the regrowth interface before and after process optimization is shown in Fig. S3a and b, respectively. More details about the optical gain measurements of the QD active region are available in Refs. [2, 3].

## II. LINEWIDTH ENHANCEMENT FACTOR

The linewidth enhancement factor (LEF) is measured by using the amplified spontaneous emission (ASE) method [4]. Compared to the high-speed frequency and amplitude modulation method [5], the ASE method allows for direct measurement of the differential gain and differential refractive index as a function of the carrier density in sub-threshold operation. The differential refractive index $dn/dN$ is measured by tracking the wavelength shift of the DFB mode, while its differential gain $dg/dN$ is extracted by tracking the variation of the net modal gain $G_{net}$. The net modal gain is measured by the DFB modulation depth (gain ripple) from the ASE spectra, which is calculated by using the following relationship [6]:

$$G_{net} = \frac{1}{L_c} ln(\frac{1}{\sqrt{R_1 R_2}} \frac{\sqrt{x}-1}{\sqrt{x}+1}) \tag{1}$$

where $L_c$ is cavity length, $R_1$ and $R_2$ denote the power reflectivities of the front and the rear facets, respectively. $x$ accounts for the ratio of the peak-to-valley intensity levels. The differential refractive index within the active region can be calculated by the modal wavelength shift $d\lambda_m$ through $d\lambda_m/\lambda_m$=$\Gamma dn/n$, with $\lambda_m$ and $\Gamma$ the modal wavelength

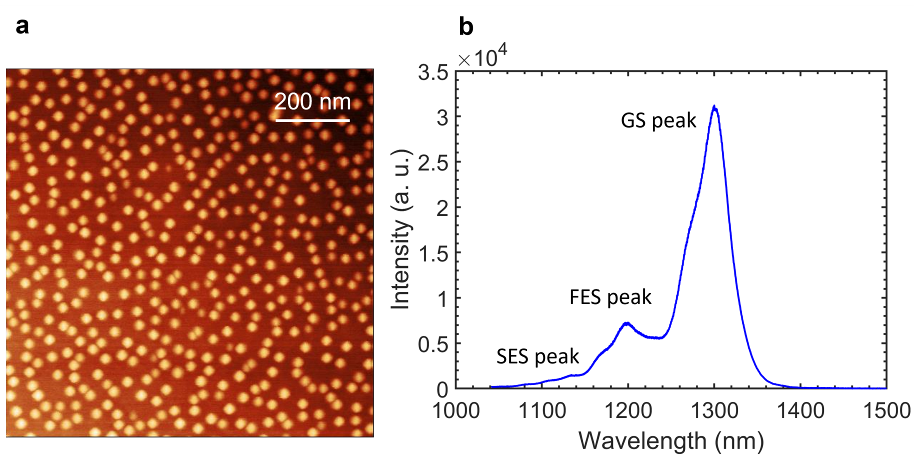


**Supplementary Figure** 1. **Characterizations of the QD active region. a** The atomic force microscopy (AFM) scan of the exposed surface dots, where the surface dot density is $6{\times}10^{10}$cm$^{-2}$. **b** Room-temperature PL spectrum of InAs QDs grown on a GaAs/Si substrate, with a ground state peak wavelength of 1293 nm.

and the optical confinement factor, respectively. Therefore, the LEF is extracted using the following relationship:

$$\alpha_H = -\frac{4n\pi}{\lambda_m^2}\frac{d\lambda_m/dI}{dG_{net}/dI} \tag{2}$$

The optical spectrum at twice the threshold current of the wavelength-detuned QD laser is shown in Fig. S4a. The QD laser is operating at 1323 nm, and its LEF is then measured by tracking the net modal gain and lasing wavelength versus the normalized gain current (Fig. S4b and c). The net modal gain increases with gain current below the threshold until it clamps the mirror loss above the threshold. Nevertheless, it should be noted that the thermal effect also contributes to a wavelength shift, which could possibly lead to an underestimation of the LEF. While the wavelength shift below the threshold $d\lambda_{m,b}$ results from both the carrier-induced refractive index change and the thermal effect, the wavelength shift above the threshold $d\lambda_{m,a}$ is mainly caused by the thermal effect since the gain is clamped. The sub-threshold and above-threshold wavelength shifts are expressed as follows:

$$d\lambda_{m,b} = (\frac{dn}{n} + \frac{dn_t}{n} + \frac{dL_t}{L_t})\lambda_m \tag{3}$$

$$d\lambda_{m,a} = (\frac{dn_t}{n} + \frac{dL_t}{L_t})\lambda_m \tag{4}$$

where $dn_t$ accounts for the refractive index change due to the thermal effect, and $dL_t$ denotes the thermal expansion of the laser cavity. Eq. (2) can be then reexpressed as follows:

$$\alpha_H = -\frac{4n\pi}{\lambda_m^2}\frac{(d\lambda_{m,b} - d\lambda_{m,a})/dI}{dG_{net}/dI} \tag{5}$$

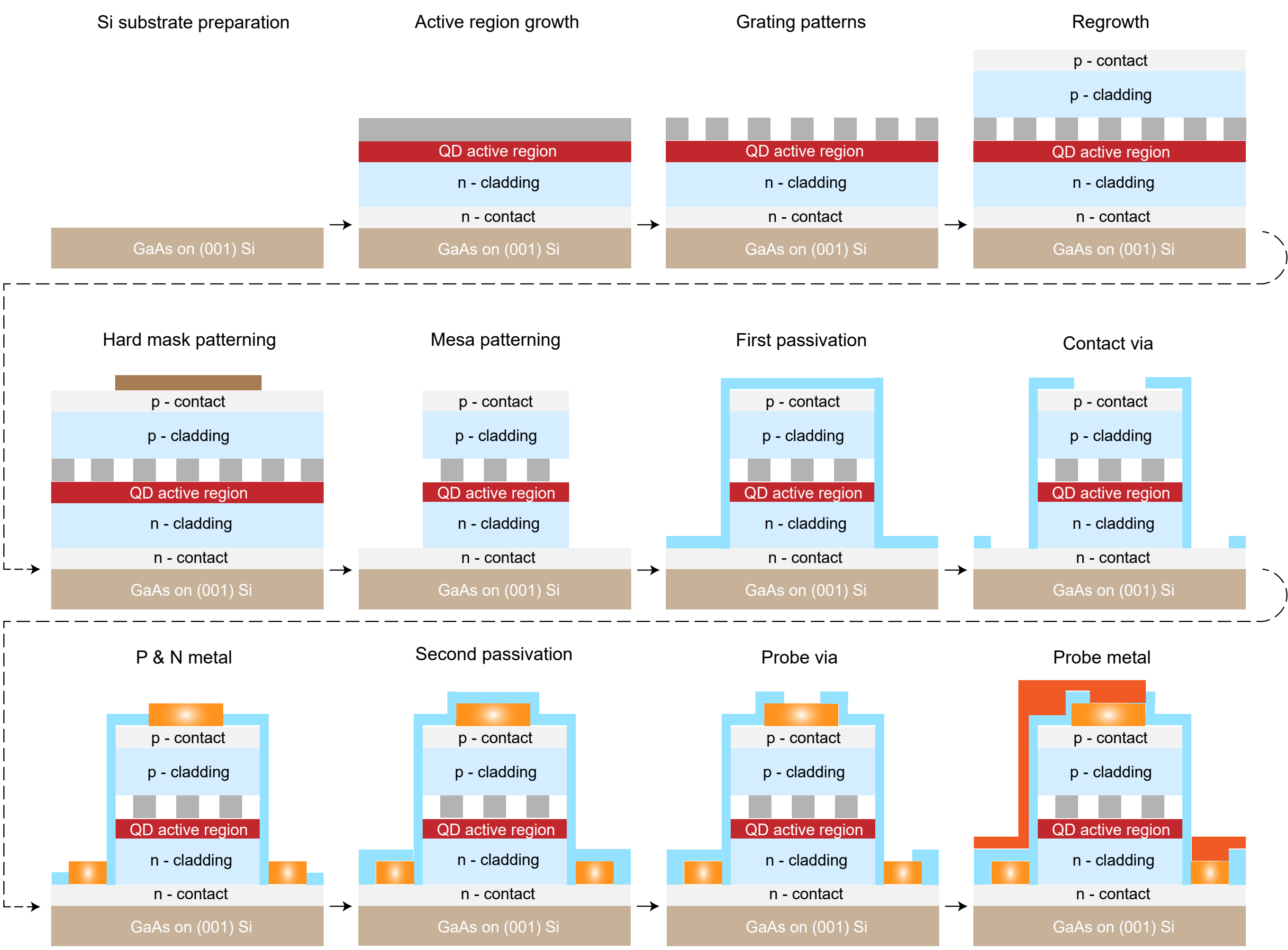


**Supplementary Figure 2. Full QD laser processing flow.**

| Layer | Material | Thickness (nm) | Doping ($cm^3$) | Function |
|---|---|---|---|---|
| 1 | P-GaAs | 300 | $1.5\times10^{19}$ | P-contact |
| 2 | P-$Al_xGa_{1-x}As$ | 50 | $3\times10^{18}$ | Smoothing |
| 3 | P-$Al_{0.4}Ga_{0.6}As$ | 1400 | $5\times10^{17}$ | P-cladding |
| 4 | P-$Al_xGa_{1-x}As$ | 50 | $3\times10^{18}$ | Smoothing |
| 5 | GaAs | 100 | UID | Grating |
| 6 | GaAs | 12.5 | UID | Smoothing |
| 7 | 5×GaAs | 37.5 | $5\times10^{17}$ | Spacing |
| 8 | 5×InAs | 7 | UID | QD |
| 9 | GaAs | 50 | UID | Smoothing |
| 10 | N-$Al_xGa_{1-x}As$ | 50 | $3\times10^{18}$ | Smoothing |
| 11 | N-$Al_{0.4}Ga_{0.6}As$ | 1400 | $5\times10^{17}$ | N-cladding |
| 12 | N-$Al_xGa_{1-x}As$ | 50 | $3\times10^{18}$ | Smoothing |
| 13 | N-GaAs | 1000 | $1.5\times10^{19}$ | N-contact |
| 14 | GaAs | 500 | UID | Buffer |
| 15 | $In_{0.1}Ga_{0.9}As$ | 200 | UID | Buffer |
| 16 | GaAs | 500 | UID | Buffer |
| 17 | GaP | 45 | UID | Smoothing |
| 18 | Si | - | UID | Substrate |

Table I. The stack information of InAs/GaAs QD on Si epi, from the top (layer 1) to the bottom (layer 18). UID: unintentionally doped.

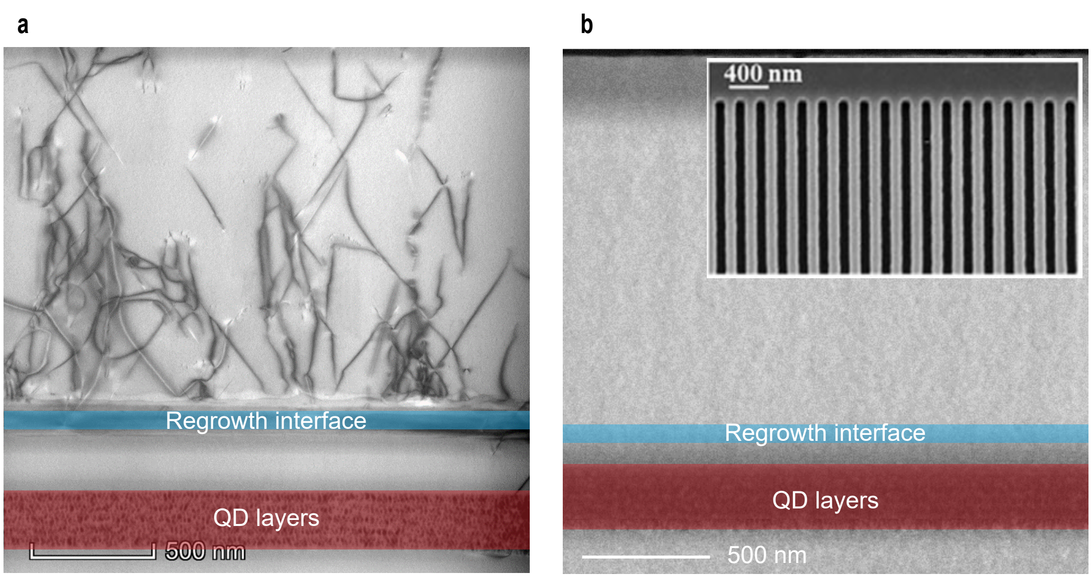


**Supplementary Figure** 3. **Optimization of the regrowth process**. **a**. TEM image of the active region before the optimization of the regrowth. Massive amount of crystalline defects were observed in the p-cladding layers. **b**. TEM image of the active region after the optimization of the regrowth. Predestine crystalline quality was obtained with minimum detectable defects.

where the thermal effect is eliminated in the measurements of LEF. As a result of the wavelength detuning of 12 nm, the LEF of the QD laser is increased to 2.6.

The optical spectrum at twice the threshold current, the net modal gains, and the wavelength shift of the commercial QW laser are shown in Figs. S4d-f, respectively. The Bragg wavelength of the QW laser is located at the optical gain peak, which enables the intrinsic LEF of the QW. The measured LEF is 3.3, which is a typical value for a QW laser.

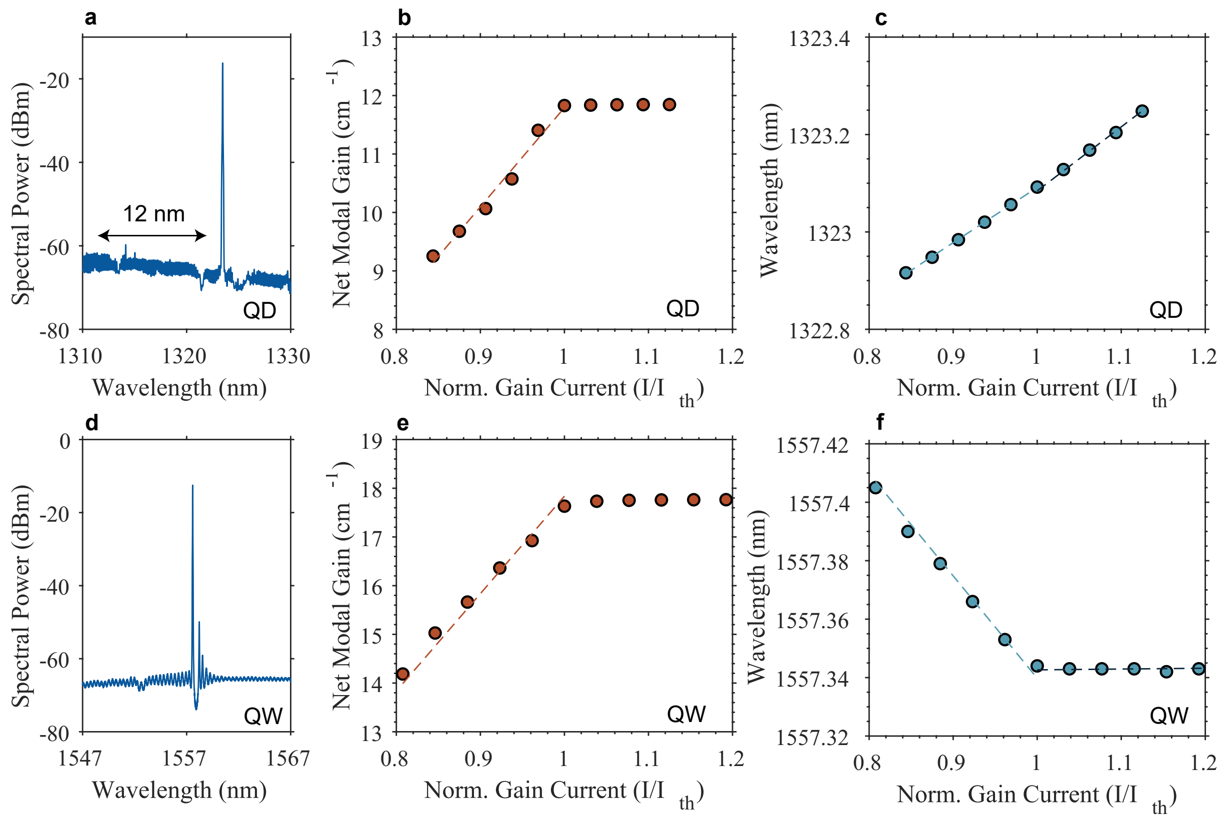


**Supplementary Figure** 4. **Linewidth enhancement factor measurements**. **a**. Optical spectrum at twice the threshold current of the wavelength-detuned QD laser. **b**. Net modal gain $G_{net}$ as a function of the normalized gain current of the QD laser. **c**. Modal wavelength $\lambda_m$ as a function of the normalized gain current of the QD laser. **d**. Optical spectrum at twice the threshold current of the QW laser. **e**. Net modal gain $G_{net}$ as a function of the normalized gain current of the QW laser. **f**. Modal wavelength $\lambda_m$ as a function of the normalized gain current of the QW laser.

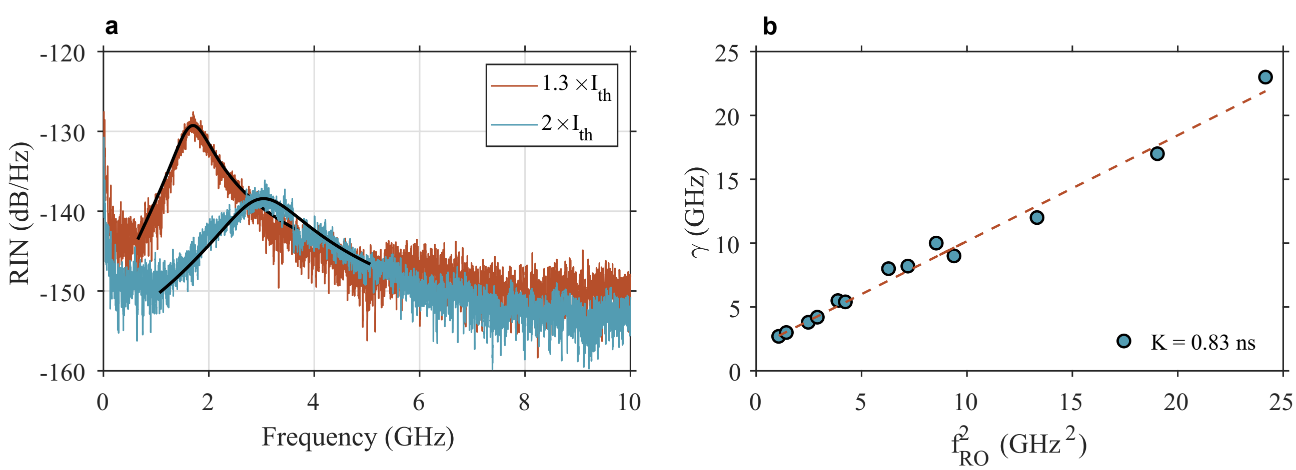


**Supplementary Figure** 5. **Relaxation oscillation frequency and damping factor measurements of a commercial QW laser**. **a**. Relative intensity noise (RIN) at $1.3\times I_{th}$ (burgundy) and $2\times I_{th}$ (jade) at room temperature (20°C). **b**. Damping factor as a function of the squared relaxation oscillation frequency (ROF).

## III. RELAXATION OSCILLATION FREQUENCY AND DAMPING FACTOR

Both the relaxation oscillation frequency $f_{RO}$ (ROF) and the damping factor $\gamma$ are retrieved from the relative intensity noise (RIN) spectrum. Here we take the case of the QW laser as an example. Figure S5(a) depicts the RIN spectra at $1.3\times I_{th}$ (burgundy) and $2\times I_{th}$ (jade) at room temperature (20°C). An increase in the gain current increases both the ROF and the damping factor, in the presence of the decrease in the amplitude of ROF. A curve-fitting as the following relationship allows us to obtain these two parameters independently [7]:

$$RIN(\omega) = \frac{a + b\omega^2}{(\omega^2 - \omega_{RO}^2)^2 + \omega^2\gamma^2} \tag{6}$$

where $\omega_{RO}$ denotes the angular frequency of the ROF and $\omega$ is the angular frequency. $a$ and $b$ are the coefficients used for the curve-fitting.

On the other hand, the $K$-factor is also a well-known parameter in the small-signal frequency response that describes the damping, which is directly determined by the ROF and the damping factor through the following relationship:

$$\gamma = Kf_{RO}^2 + \gamma_0 \tag{7}$$

with $\gamma_0$ the damping factor offset. Figure S5(b) displays the damping factor as a function of the squared ROF. The retrieved $K$-factor is 0.83 ns, which is a typical value for a QW laser. On the contrary, the damping factor is much larger in the QD laser, which contributes to the suppression of the ROF [7]. In this work, the $K$-factor of the wavelength-detuned QD laser is larger than 5 ns given that the ROF is fully suppressed.

## IV. FEEDBACK SENSITIVITY AND LINEWIDTH REDUCTION IN SEMICONDUCTOR LASER

In general, semiconductor laser diodes are sensitive to external optical feedback due to their class B nature. The classification of a laser system depends on the photon lifetime $\tau_p$, the carrier lifetime $\tau_c$, and the polarization lifetime $\tau_{pol}$. A class B laser obeys $\tau_c \geq \tau_p \gg \tau_{pol}$. As explained in Ref. [8], an additional degree of freedom such as Q-switching, optical injection, and optical feedback is able to trigger novel dynamics from those lasers. The process of back reflection is to send part of the laser's emitted field back to the laser cavity. Therefore, two important parameters are related to this process. The first one is the feedback strength, whose definition has been introduced in the main text (Methods). The other one is the external cavity length $L_{ext}$ that corresponds to the external round-trip time $\tau_{ext}$, which is expressed as:

$$\tau_{ext} = \frac{2L_{ext}}{v_g} \tag{8}$$

where $v_g$ denotes the group velocity in the external cavity.

When a semiconductor laser is subject to external optical feedback, the amplitude-phase coupling between the returned field and the intracavity one is described by the field fluctuations in the amplitude and the phase. The perturbation of the photon density due to the returned field contributes to a fluctuation of both the carrier density and the optical gain. The latter, which is attributed to the damping effect, changes the refractive index through the LEF and results in a wavelength shift. On the other hand, the returned field will lead to an additional wavelength shift through the phase fluctuation. As a result, the interaction of the intensity and the phase results in complex nonlinear dynamics when the laser is subject to back reflection. Stable and unstable laser dynamics including linewidth reduction, periodic oscillation, coherence collapse, or low-frequency fluctuations can be triggered [9].

To analyze the feedback sensitivity of laser diode, one of the commonly used definitions of the $r_{crit}$ is written as follows [10]:

$$r_{crit} = \frac{\tau_{in}(Kf_{RO}^2 + 1/\tau_{ext})^2}{16C_l^2}\left(\frac{1+\alpha_H^2}{\alpha_H^4}\right) \tag{9}$$

where $\tau_{in}$ and $C_l$ are the round-trip time of the laser cavity resonance and the coupling coefficient from the laser cavity to the external cavity, respectively. The latter can be roughly determined by $C_l$=$(1-R)/\sqrt{R}$ where R accounts for the facet power reflection. Eq. (9) gives a quantitative description of the feedback sensitivity of a semiconductor laser. The 35 dB improved feedback insensitivity in the wavelength-detuned QD laser is attributed to its much stronger damping factor and relatively lower LEF than its QW counterpart. The former contributes to a decrease in the gain fluctuation; the latter allows for efficiently decoupling the photon density fluctuation and the frequency shift. On the other hand, the feedback sensitivity becomes quasi-independent of the external cavity length in the long-cavity regime where the laser ROF is much larger than the external cavity frequency [11].

Depending on the feedback strength, Tkach and Chraplyvy defined five feedback regimes for a DFB laser diode [12]. A laser diode is unconditionally stable against back reflection in Regime I. As the feedback strength increases, in-phase external feedback enables linewidth narrowing in Regime II, and the narrowest linewidth is achieved in Regime III. Nevertheless, strong enough external feedback destabilizes the laser, and coherence collapse takes place in Regime IV. Some unstable laser sources, i.e., bulk laser diodes, can be restabilized in Regime V once the feedback strength is further improved. Nevertheless, this regime is very difficult to reach since the feedback strength is usually limited by the facet reflection.

To take advantage of the narrow-linewidth operation in Regimes II and III, it is crucial to suppress Regime IV. This used to be a challenge in the conventional QW lasers since they are easily destabilized by weak external feedback. The critical feedback level for the commercial QW laser studied is -37 dB, which is not favorable to the linewidth reduction by using an external cavity without a frequency filter. On the contrary, the chaos-free operation offered by the QD laser addresses the issue of Regime IV and allows for linewidth reduction by using a low-Q external cavity. The increased LEF due to the wavelength detuning also enables a giant linewidth reduction.

## V. THEORY OF LASER EXTERNAL CAVITY LOCKING

Dynamics of the DFB laser under external cavity locking are described by the Van der Pol equation (10) for the complex electric field $E(t) = |E(t)|e^{i\phi(t)}$ with an additional feedback term $\kappa E(t-\tau_{ext})$ which describes the light coupled back into the laser cavity, and equation (11) describing dynamics of the carrier density $N(t)$ [13–15]:

$$\dot{E}(t) = \left[-i\omega_0 + \frac{1}{2}\left(G(t) - \frac{1}{\tau_p}\right)(1 - i\alpha_H)\right]E(t) + \kappa E(t-\tau_{ext})e^{-i\omega_0\tau_{ext}} + \mathcal{F}_E(t) \tag{10}$$

$$\dot{N}(t) = \frac{I}{eV} - \frac{N(t)}{\tau_c} - G(t)|E(t)|^2 \tag{11}$$

where the gain $G(t) = \Gamma g_0 \frac{N_0 ln(N(t)/N_0)}{1+\varepsilon|E(t)|^2}$, $\omega_0$ is the laser angular frequency, $\tau_c$ and $\tau_p$ are the carrier and photon lifetimes, respectively, $\alpha_H$ is the linewidth enhancement factor, $\tau_{ext}$ is the round-trip time in the external cavity comprised of the optical fiber and back reflector, $I$ is the injection current, $g_0$ is the differential gain coefficient, $\varepsilon$ is the gain compression factor, $N_0$ is the transparency carrier density, $e$ is the electron charge, $V$ is the active medium volume, while $\Gamma$ is the confinement factor. The feedback coefficient $\kappa$ is a key factor in describing the optical feedback mechanism and is given as:

$$\kappa = \frac{2C_C\sqrt{\eta_f}}{\tau_L} \tag{12}$$

where $\eta_f$ is the feedback strength, $\tau_L$ is the laser cavity roundtrip time, while $C_C$ is the coupling strength coefficient, which for an AR/HR DFB laser is given by [16]:

$$C_C = \frac{2(1-R_1)(q^2+\kappa_0^2)L^2}{i\kappa_0 L(1+R_1) - 2qL\sqrt{R_1}} \times \left[\frac{1}{2qL - \sum_{k=1}^{2}\frac{1-R_k\kappa_0 L}{2iqL\sqrt{R_k}+\kappa_0 L(1+R_k)}}\right] \tag{13}$$

In equation (13), $R_1$ and $R_2$ are the power reflectivities of the AR and HR facets, respectively, $\kappa_0$ is index-coupling coefficient of the DFB structure, $L$ is the length of the laser cavity, and $q = \alpha_0 - i\delta_0$ with $\alpha_0$ and $\delta_0$ respectively being the laser losses and the Bragg deviation, both for the free-running case (without optical feedback). The white noise effect of spontaneous emission on the laser dynamics is described by the Langevin noise source $\mathcal{F}_E(t)$ [17]. The number of noise events follows a Poisson distribution $\mathcal{P}(\lambda_N)$ with a mean of $\langle\lambda_N\rangle = R_{sp}\Delta t$, $\Delta t$ being the simulation time step, and $R_{sp}$ is the spontaneous emission rate, given as:

$$R_{sp} = \beta_{sp}\frac{N_{ss}}{\tau_c} \tag{14}$$

where $\beta_{sp}$ is the spontaneous emission factor and $N_{ss}$ is the steady-state carrier density. The white noise term $\mathcal{F}_E(t)$ itself follows a Gaussian distribution $\mathcal{N}(0,\sigma_E^2)$ with a mean of zero [17–19], and a standard deviation $\sigma_E = \sqrt{\langle\lambda_N\rangle/2V}$ [20]. In other words,

$$\mathcal{F}_E = \sqrt{\frac{\beta_{sp}N_{ss}}{2V\tau_c\Delta t}}\mathcal{Z}_E \tag{15}$$

where $\mathcal{Z}_E$ is a random variable sampled from the standard normal distribution $\mathcal{N}(0,1)$. In order to accurately model the simulated QW and QD lasers under test, their respective active medium parameters were experimentally extracted. Firstly, the L-I curve of each device in the free-running regime is fitted to the positive solution of [21]:

$$(\zeta P_{out})^2 - (I - I_{th} - I_s)\zeta P_{out} - I_s I \approx 0 \tag{16}$$

where $I$ is the injected current, $\zeta$ is the inverse of the slope efficiency, and $I_s$ denotes the portion of the injected current contributing to spontaneous emission. From equation (16), the threshold current $I_{th}$ as well as $\zeta$ and $I_s$ were extracted as fitting parameters. Then, the relaxation oscillation damping factor $\Gamma_{RO}$ and frequency $\Omega_{RO}$ were measured through the relative intensity noise (RIN) profile of each device at two current injection points, 1 and 2. From them, $g_0$, $\tau_p$, $\tau_c$, $\beta_{sp}$, and $N_0$ were estimated according to [22, 23]:

$$g_0 = \frac{eV\Omega^2_{RO_2}}{\Gamma(I - I_{th})} \tag{17}$$

$$\tau_p = \frac{2(\Gamma_{RO_2} - \Gamma_{RO_1})}{\Omega^2_{RO_2} - \Omega^2_{RO_1}} \tag{18}$$

$$\tau_c = \frac{1}{2\Gamma_{RO_2} - \Omega^2_{RO_2}\tau_p} \tag{19}$$

$$\beta_{sp} = \frac{\Gamma I_s g_0 \tau_p \tau_c}{eV} \tag{20}$$

$$N_0 = \frac{I_{th}\tau_c}{eV} - \frac{1}{\Gamma g_0 \tau_p} \tag{21}$$

Lastly, $\alpha_H$ was experimentally estimated following the Hakki-Paoli method based on measurements of intensity peaks of the amplified spontaneous emission (ASE) spectra of the lasers under different sub-threshold currents [24]. Using equations (10) and (11), the complex field $E(t) = |E(t)|e^{i\phi(t)}$ was computed over a period of time $T$ long enough to resolve the sub-kHz linewidths exhibited by the external cavity-locked laser. In order to accommodate the vast amount of data points required to accomplish that, computations of the complex field $E(t)$ were performed in an out-of-core fashion. Ultimately, the simulated frequency noise spectrum $S_\nu(f)$ is then calculated as:

$$S_\nu(f) = \frac{1}{T}\left|\int_0^T \Delta\nu(t)e^{-2\pi i f t}dt\right|^2 \tag{22}$$

where $\Delta\nu(t) = \nu(t) - \bar{\nu}$, $\nu(t) = d\phi(t)/dt$, and $\bar{\nu}$ is the time-averaged value of $\nu(t)$. The final frequency noise spectra shown in Figs. 3e and h in the manuscript are obtained by averaging several separately calculated frequency noise spectra $S_\nu(f)$.

---


[1] P. E. Vullum, M. Nord, M. Vatanparast, S. F. Thomassen, C. Boothroyd, R. Holmestad, B.-O. Fimland, and T. W. Reenaas, Quantitative strain analysis of InAs/GaAs quantum dot materials, Scientific reports **7**, 45376 (2017).

[2] Z. Zhang, D. Jung, J. C. Norman, P. Patel, W. W. Chow, and J. E. Bowers, Effects of modulation p doping in InAs quantum dot lasers on silicon, Applied Physics Letters **113**, 10.1063/1.5040792 (2018).

[3] J. Duan, H. Huang, D. Jung, Z. Zhang, J. Norman, J. Bowers, and F. Grillot, Semiconductor quantum dot lasers epitaxially grown on silicon with low linewidth enhancement factor, Applied Physics Letters **112**, 251111 (2018).

[4] M. Osinski and J. Buus, Linewidth Broadening Factor in Semiconductor Lasers–An Overview, IEEE Journal of Quantum Electronics **23**, 9 (1987).

[5] B. Dong, J. Duan, H. Huang, J. C. Norman, K. Nishi, K. Takemasa, M. Sugawara, J. E. Bowers, and F. Grillot, Dynamic performance and reflection sensitivity of quantum dot distributed feedback lasers with large optical mismatch, Photonics Research **9**, 1550 (2021).

[6] D. Bossert and D. Gallant, Improved method for gain/index measurements of semiconductor lasers, Electronics Letters **32**, 338 (1996).

[7] J. Duan, Y. Zhou, B. Dong, H. Huang, J. C. Norman, D. Jung, Z. Zhang, C. Wang, J. E. Bowers, and F. Grillot, Effect of p-doping on the intensity noise of epitaxial quantum dot lasers on silicon, Optics Letters **45**, 4887 (2020).

[8] F. Arecchi, R. Meucci, G. Puccioni, and J. Tredicce, Experimental evidence of subharmonic bifurcations, multistability, and turbulence in a Q-switched gas laser, Physical Review Letters **49**, 1217 (1982).

[9] J. Ohtsubo, *Semiconductor lasers: stability, instability and chaos*, Vol. 111 (Springer, 2012).

[10] J. Helms and K. Petermann, A Simple Analytic Expression for the Stable Operation Range of Laser Diodes with Optical Feedback, IEEE Journal of Quantum Electronics **26**, 833 (1990).

[11] B. Dong, J.-D. Chen, F.-Y. Lin, J. C. Norman, J. E. Bowers, and F. Grillot, Dynamic and nonlinear properties of epitaxial quantum-dot lasers on silicon operating under long-and short-cavity feedback conditions for photonic integrated circuits, Physical Review A **103**, 033509 (2021).

[12] R. Tkach and A. Chraplyvy, Regimes of feedback effects in 1.5-µm distributed feedback lasers, Journal of Lightwave Technology **4**, 1655 (1986).

[13] R. Lang and K. Kobayashi, External optical feedback effects on semiconductor injection laser properties, IEEE journal of Quantum Electronics **16**, 347 (1980).

[14] G. Agrawal, Line narrowing in a single-mode injection laser due to external optical feedback, IEEE Journal of Quantum Electronics **20**, 468 (1984).

[15] K. Kikuchi and T. Okoshi, Simple formula giving spectrum-narrowing ratio of semiconductor-laser output obtained by optical feedback, Electronics Letters **18**, 10 (1982).

[16] F. Grillot, On the effects of an antireflection coating impairment on the sensitivity to optical feedback of AR/HR semiconductor DFB lasers, IEEE Journal of Quantum Electronics **45**, 720 (2009).

[17] C. Henry, Theory of the phase noise and power spectrum of a single mode injection laser, IEEE Journal of Quantum Electronics **19**, 1391 (1983).

[18] K. Vahala and A. Yariv, Semiclassical theory of noise in semiconductor lasers-Part II, IEEE Journal of quantum electronics **19**, 1102 (1983).

[19] M. Lax, Classical noise. V. Noise in self-sustained oscillators, Physical Review **160**, 290 (1967).

[20] H. Olesen, J. Osmundsen, and B. Tromborg, Nonlinear dynamics and spectral behavior for an external cavity laser, IEEE journal of quantum electronics **22**, 762 (1986).

[21] L. Bjerkan, A. Royset, L. Hafskjaer, and D. Myhre, Measurement of laser parameters for simulation of high-speed fiberoptic systems, Journal of Lightwave Technology **14**, 839 (1996).

[22] J. C. Cartledge and R. Srinivasan, Extraction of DFB laser rate equation parameters for system simulation purposes, Journal of Lightwave Technology **15**, 852 (1997).

[23] I. Tomkos, I. Roudas, R. Hesse, N. Antoniades, A. Boskovic, and R. Vodhanel, Extraction of laser rate equations parameters for representative simulations of metropolitan-area transmission systems and networks, Optics communications **194**, 109 (2001).

[24] B. W. Hakki and T. L. Paoli, Gain spectra in GaAs double- heterostructure injection lasers, Journal of Applied Physics **46**, 1299 (1975).